frontiers | Frontiers in Marine Science

TYPE Original Research
PUBLISHED 20 October 2022
DOI 10.3389/fmars.2022.1022957

OPEN ACCESS

EDITED BY
Susana Agusti,
King Abdullah University of Science and Technology, Saudi Arabia

REVIEWED BY
Sarat Chandra Tripathy,
National Centre for Polar and Ocean Research (NCPOR), India
Anastazia T. Banaszak,
National Autonomous University of Mexico, Mexico

*CORRESPONDENCE
Elliot L. Weiss
eweiss@ucsd.edu

SPECIALTY SECTION
This article was submitted to Aquatic Microbiology, a section of the journal Frontiers in Marine Science

RECEIVED 19 August 2022
ACCEPTED 04 October 2022
PUBLISHED 20 October 2022

CITATION
Weiss EL, Cape MR, Pan BJ, Vernet M, James CC, Smyth TJ, Ha S-Y, Iriarte JL and Mitchell BG (2022) The distribution of mycosporine-like amino acids in phytoplankton across a Southern Ocean transect. *Front. Mar. Sci.* 9:1022957. doi: 10.3389/fmars.2022.1022957

The distribution of mycosporine-like amino acids in phytoplankton across a Southern Ocean transect

Elliot L. Weiss[1*], Mattias Rolf Cape[2], B. Jack Pan[3], Maria Vernet[1], Chase C. James[1], Tim J. Smyth[4], Sun-Yong Ha[5], José L. Iriarte[6] and B. Greg Mitchell[1]

[1]Scripps Institution of Oceanography, University of California, San Diego, San Diego, CA, United States, [2]School of Oceanography, University of Washington, Seattle, WA, United States, [3]Jet Propulsion Laboratory, California Institute of Technology, Pasadena, CA, United States, [4]Plymouth Marine Laboratory, Plymouth, United Kingdom, [5]Division of Polar Ocean Science, Korea Polar Research Institute, Incheon, South Korea, [6]Centro de Investigación IDEAL - Dinámica de Ecosistemas Marinos de Altas Latitudes, and Instituto de Acuicultura, Universidad Austral de Chile, Puerto Montt, Chile

Interactions between phytoplankton and ultraviolet radiation (UVR: 280 – 400 nm) are undergoing changes dictated by variability in ocean temperature, the depth of mixed layers, nutrient availability, and the thickness of the ozone layer. There are a variety of mechanisms for phytoplankton to cope with UVR stress, one of the most prevalent being the presence of mycosporine-like amino acids (MAAs). Despite the importance of these molecules to phytoplankton fitness under UVR stress, knowledge of the diversity and distribution of these molecules in the world's oceans is relatively limited. Here, the composition and distribution of MAAs in phytoplankton were examined in a transect across the Southern Ocean, crossing multiple fronts, from eastern New Zealand to the West Antarctic Peninsula in March and April of 2018. The highest concentration of MAAs (> 0.2 μg/L) was found between 50 and 60°S, as well as along a longitudinal gradient between 137.47 and 144.78°W. A strong correlation was found between a model of the preceding month's UVR dosage experienced in the mixed layer and the ratio of MAAs to chlorophyll-a across the transect, indicating a relationship between the integrated history of light exposure and phytoplankton physiology. Haptophytes accounted for the majority of biomass north of the polar front (PF) and were strongly correlated with a diversity of MAAs. South of the PF a transition to a community dominated by diatoms was observed, with community composition changes strongly correlated to porphyra-334 concentrations. The data presented here provide a baseline for MAA abundance and association with specific phytoplankton taxa across the Southern Ocean amid a changing climate.

KEYWORDS

mycosporine-like amino acids, ultraviolet radiation, Southern Ocean, phytoplankton, diatoms, UV-absorbing compounds, MAAs, sunscreens

Introduction

Ultraviolet radiation (UVR: 280 – 400 nm) is the most photochemically reactive waveband of the incident solar radiation field and has profound effects on the physiology of organisms living at or near the Earth's surface (Cullen and Neale, 1994; Vincent and Neale, 2000; Häder and Gao, 2015). In aquatic environments, interactions between climate change, the ozone layer, and UVR are continually modulating the length of exposure of aquatic organisms to UVR as well as the spectral quality and balance of incident radiation (Erickson et al., 2015; Barnes et al., 2019). Changes in UVR exposure alter the physiology and productivity of phytoplankton, which likely have cascading effects throughout ecosystems (De Mora et al., 2000). Climate change and other environmental variables will play a large role in the exposure of aquatic organisms to UVR. The shoaling of upper mixed layers (UML) in some oceanic regions due to increased water temperature, and deepening of the UML in others due to intensification of surface turbulence (Sallée et al., 2021), will alter the dosage of UVR received by pelagic organisms. Additionally, increases in melting of glaciers and permafrost are increasing coastal dissolved organic matter (DOM) levels thereby enhancing UVR absorption, while prolonged exposure of DOM to UVR in shoaled mixed layers may enhance DOM bleaching (Barnes et al., 2019; Hood et al., 2020). While these processes undergo natural cycles, projections from climate change modelling experiments predict that stratification will increase and the depth of the UML will be altered in the Southern Ocean (Constable et al., 2014; Sallée et al., 2021), resulting in changes in UVR dosages experienced by phytoplankton. Updated climate models, such as RCP-6.0, indicate that the Antarctic ozone hole is expected to close, with springtime ozone levels returning to 1980 values by 2060 (World Meteorological Organization (WMO), 2018). However, recovery rates depend on continued compliance with the Montreal Protocol and recent findings of increased emission of chlorofluorocarbon-11 from eastern Asia and relatively short-lived chloroform emissions from China, among others, may delay ozone recovery (Fahey et al., 2018; Fang et al., 2019; Harris et al., 2019). Indeed, recent springtime UVR measurements along the Antarctic Peninsula nearing peak levels observed more than two decades ago suggest that UVR exposure remains a significant environmental stressor for the marine environment (Cordero et al., 2022).

UVR has both direct and indirect mechanisms of damage to photosynthetic biota. Mechanisms are manifested in damage to DNA, proteins, pigments, inhibition of photosynthesis, nitrogen fixation, retardation of nutrient uptake and cell motility, and the formation of reactive oxygen species (De Mora et al., 2000). Photosynthetic organisms have continued to develop an array of coping strategies to minimize the direct and indirect damage from UVR such as avoidance of UVR *via* cilia, flagella, or buoyancy regulation, DNA repair, the production of antioxidants, the recycling and repair of damaged proteins, and/or the synthesis of photoprotective pigments and intracellular or extracellular sunscreen molecules (Häder et al., 2015).

Mycosporine-like amino acids (MAAs) are one such type of sunscreen molecule, widely distributed in terrestrial, freshwater, and marine environments, and found in many types of organisms such as bacteria, fungi, the ocular lenses of fish, and are frequently part of an overall strategy of phytoplankton to diminish the inimical effects of UVR (Lesser, 1996; Moisan and Mitchell, 2001; Shick and Dunlap, 2002; Núñez-Pons et al., 2018). MAAs are one of the strongest UVR absorbing natural products (molar extinction coefficients ranging from 28,100–50,000 M^{-1} cm^{-1}), which are characterized by their low molecular weight, high solubility and polarity and are composed of a cyclohexenone or cyclohexenimine chromophore conjugated to an amino acid or its amino alcohol, with absorption maxima ranging from 310 to 362 nm (Schmid et al., 2004; Sinha et al., 2007; Wada et al., 2015; Orfanoudaki et al., 2019). MAAs act as an effective sunscreen against photo-inhibition and provide a defense against the photooxidative stress of UVR (Carreto and Carignan, 2011). In addition to their role as a sunscreen, certain MAAs have been assigned antioxidant activity and roles in osmoregulation (Portwich and Garcia-Pichel, 1999; Rastogi and Incharoensakdi, 2014). The synthesis of MAAs can be induced by exposure to UVR, far-red light, high levels of visible light, and modulated by osmotic conditions as well as nutrient limitation (Portwich and Garcia-Pichel, 1999; Moisan and Mitchell, 2001; Llewellyn et al., 2020).

Patterns of MAA production in the environment may serve as bioindicators of UVR-induced stress in phytoplankton, as has been suggested for patterns of DNA-damage and pigmentation in zooplankton (Hessen, 1993). Indeed, observed variability in MAA production as a function of season (i.e., summer peak) and depth (surface maximum) suggest a tight coupling between the magnitude of UVR forcing and physiological response in phytoplankton and other marine organisms (Morrison and Nelson, 2004; Núñez-Pons et al., 2018 and references therein), while the inability of certain species to produce MAAs imply that UVR may act as a forcing on phytoplankton community composition (Ha et al., 2018; Núñez-Pons et al., 2018). In the future, absorption of UVR by MAAs may enhance satellite taxonomic characterization *via* remote sensing of UVR spectral bands (Kahru and Mitchell, 1998; Kahru et al., 2021). Recently, Kahru et al. (2021) demonstrated that remote detection using UVR spectral bands was able to differentiate neighboring algal blooms of differing taxonomic composition, likely due to the presence of MAAs. Various studies have been conducted to assess phytoplankton MAA composition in coastal marine and freshwater systems and in laboratory cultures (Whitehead and Vernet, 2000; Llewellyn and Harbour, 2003; Carreto et al., 2018), yet little is known about the abundance and composition of MAAs throughout the world's oceans, as few studies have been conducted on large spatial scales. Such larger scale studies in existence include the Sub-Antarctic Zone south of Tasmania in 2007 (Oubelkheir et al., 2013),

and a latitudinal gradient across the Atlantic Ocean in 2008 (Llewellyn et al., 2012). An enhanced understanding of the global distribution of MAAs, the chemotaxonomic association of MAAs with phytoplankton, and the dynamics between MAA biosynthesis and abiotic factors such as UVR dosage will help to inform remote sensing observations as more satellites are equipped with ocean color sensors in the UVR region. Additionally, an understanding of the utility of MAAs to serve as bio-indicators of UVR-induced stress may help to improve ecosystem and biogeochemical models that incorporate spectral light and explicit radiative transfer to examine the role of the irradiance spectrum and pigments in establishing the biogeography of phytoplankton (Dutkiewicz et al., 2015). In this study, we provide the first continuous assessment of surface MAA composition and abundance across the Southern Ocean, in a transect from New Zealand to the West Antarctic Peninsula (WAP), and highlight correlations between MAA composition, phytoplankton taxonomy, and modeled UVR dosage in the upper mixed layer.

Methods

Transect description and sample collection

Surface samples were collected along a transect from 54.0233°S, 176.0422°W to 62.1282°S, 56.1329°W between 3/29/18 and 4/16/18 from the icebreaker RVIB Araon, during the 2018 ANA08D expedition of the Korean Polar Research Institute (KOPRI) from Christchurch, New Zealand to the WAP. The cruise track and sampling locations are illustrated in Figure 1. Discrete seawater samples were collected from the ship's uncontaminated seawater system, with intake located at 7 m depth. Sampling occurred both at regular intervals (every 12 hours), as well as at higher resolution along major hydrographic transitions. Transitions were identified using underway sea surface salinity and temperature observations collected using a Seabird Scientific SBE45 Thermosalinograph connected to the flow-through system, as well as satellite imagery of surface chlorophyll-a and sea surface temperature using Moderate Resolution Imaging Spectroradiometer (MODIS) satellite data. Additional samples were collected when crossing climatological (average) locations of sea surface fronts (Orsi et al., 1995).

Nutrients

At selected stations, samples for analysis of dissolved nutrients (silicate, nitrate, nitrite, phosphate, and ammonia) were collected from the ship's clean flow-through system. Samples were filtered (0.45 µm) into 20 ml high density polyethylene (HDPE) scintillation vials previously cleaned in the laboratory with 10% HCl. Samples were immediately frozen at -20 C and shipped to the University of Washington, where they were analyzed within 30 days of the end of the cruise at the Marine Chemistry Laboratory in the University of Washington's School of Oceanography. Samples were analyzed using segmented flow analysis following standard protocols of Hydes et al. (2010) using a Seal Analytical AA3 AutoAnalyzer (Hood et al., 2010).

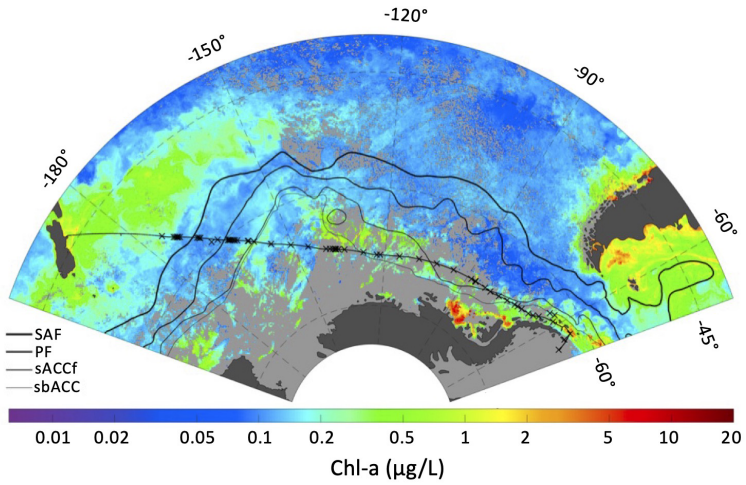

FIGURE 1
ANA08D 2018 expedition cruise track (thin black line linking New Zealand to the Antarctic Peninsula), sampling locations (x), and climatological front locations defined by Orsi et al., 1995 (SAF, Sub-Antarctic front; PF, Polar front; sACCf, Southern Antarctic Circumpolar Current font; sbACC, Southern Boundary of the ACC) overlaid on a MODIS chlorophyll-a composite for March 2018.

HPLC analysis of pigments

Phytoplankton from 0.5 to 2 L of seawater were filtered onto Whatman GF/F glass-fiber filters (25 mm diameter) using a vacuum of less than 0.5 atm. All samples were frozen on liquid nitrogen prior to shipment and extraction. Chlorophylls and carotenoids were extracted in 2 ml of 90% acetone, sonicated on ice (35 s), left to extract for 24 hours at 4°C, and filtered through Whatman Puradisc Polypropylene Syringe Filters (0.45 µm) prior to analysis. Extracted samples were run on an Agilent 1260 Infinity II LC system, with a chilled autosampler and a diode array detector operated at 450 nm, with a reverse-phase C18 column following the protocol of Zapata et al. (2000). Detected peaks were compared to known standards based on retention time and UV-visible spectra. Pigment standards were obtained from DHI, Denmark, with the exception of chlorophyll-a (chl-a) and chlorophyll-b, which were obtained from Sigma-Aldrich.

HPLC analysis of mycosporine-like amino acids

Phytoplankton from 0.5 to 2 L of seawater were filtered onto Whatman GF/F glass-fiber filters (25 mm diameter) using a vacuum of less than 0.5 atm. All samples were frozen on liquid nitrogen prior to shipment and extraction. MAAs were extracted and analyzed according to the HPLC method of Carreto et al. (2005). In brief, each sample was extracted sequentially (x3) in 2 ml of 80% methanol and sonicated on ice (30 s total, 10 s on, 5 s off). Extracts were centrifuged and pooled to remove filter debris, and the supernatant was evaporated using a Labconco Centrivap Concentrator at 30°C. Samples were resuspended in 0.5 ml of HPLC grade H_2O and filtered through a Pall Nanosep 100k Omega centrifugal filters prior to analysis. Samples were analyzed using the reverse C18 columns and the gradient elution described in Carreto et al. (2005). MAA identities were confirmed for dominant MAAs using retention times, UV-visible spectra, and LC-MS analysis. MAAs were quantified using response factors (ng/HPLC peak area) from MAAs isolated and verified by LC-MS from cultures using published extinction coefficients. For MAAs unavailable from phytoplankton cultures, HPLC eluate from similar field samples was captured, pooled and analyzed by LC-MS. The HPLC eluate was electrospray ionized (35 eV) and analyzed for positive ions using a Thermo-Finnigan LCQ Advantage ion trap mass spectrometer, fitted with an Ion-Max ESI source and run with a scanning range of 50–500 *m/z*. LC-MS column and solvent conditions were identical to HPLC analysis with the exception that the LC-MS column was not temperature controlled.

CHEMical TAXonomy analysis

Phytoplankton community composition was determined by using the CHEMical TAXonomy (CHEMTAX) software (Mackey et al., 1996), a program that uses factor analysis and a steepest descent algorithm to determine the best fit to the data with a given input matrix of pigment ratios. Using an iterative process for a given input matrix, the software optimizes the pigment ratios for each group and applies the final ratio to the total chl-a in each sample to determine the proportion of total chl-a attributed to each phytoplankton group in the community. For this study, the Microsoft Excel based CHEMTAX 1.95 with ChemtaxHelper V 7.1 was used.

The initial pigment ratios used for the CHEMTAX program (Table 1A) were adopted from Wright et al. (1996). These ratios were chosen as they have been optimized to represent the taxonomic groups found across fronts in the Southern Ocean from -45 to -65°S, a latitudinal gradient encompassing this study. All samples were analyzed together as opposed to separate bins, justified by collection from identical depths and limited samples size. Following the recommendation of established methods (Latasa, 2007), six sets of ten CHEMTAX runs each were made from the dataset, with the first runs using initial ratios found in Table 1A and up to a 75% random error added to the initial ratio values. Each subsequent run applied the output ratio of the previous run as its initial ratio, and the output calculated from the tenth run was considered final (Table 1B). Phytoplankton community data in this study are presented as relative abundance, which was calculated as each discrete sample's taxon-specific chl-a normalized by that sample's total chl-a concentration.

UVR Dosage Modelling

The UVR dosages at 305, 325, 340, and 380 nm were modeled for our discrete sampling sites using the methods of Smyth (2011), with updates to the sources of cloud data and the absorption at 443 nm as follows. Data were determined using the LibRadTran model (v1.4) using ozone, cloud-cover (extracted from the ECMWF ERA5 dataset) and Aerosol Optical Thickness as ancillary datasets, from which daily fields at ~1° resolution were calculated for 2018. Monthly composites were created, and total absorption at 443 nm (determined using Lee et al., 2005 QAA model) was used to determine the diffuse attenuation coefficient at 305, 325, 340 and 380 nm from empirical data (see Smyth (2011)). Using the mixed layer depth climatology of de Boyer Montégut et al. (2004), mixed layer depth integrated dosages were calculated. See Smyth, 2011 for full details.

TABLE 1A Initial CHEMTAX pigment ratios adopted from Wright et al. (1996).

	PER	BUT	FUCO	HEX	NEO	PRAS	VIOL	ALLO	LUT	ZEA	CHLB	CHLA
Dinoflagellates	0	0	0	0	0.15130	0.16076	0.09929	0	0.00946	0	0.94563	1
Cryptophytes	1.06186	0	0	0	0	0	0	0	0	0	0	1
Cryptophytes	0	0	0	0	0	0	0	.22850	0	0	0	1
Haptophytes-N	0	0.02548	0.09979	1	0	0	0	0	0	0	0	1
Haptophytes-S	0	0.04492	0.40430	0.50586	0	0	0	0	0	0	0	1
Chlorophytes	0	0	0	0	0.06369	0	0.05414	0	0.20223	0.00955	0.26274	1
Cyanobacteria	0	0	0	0	0	0	0	0	0	0.34771	0	1
Diatoms	0	0	0.6	0	0	0	0	0	0	0	0	1

PER, peridinin; BUT, 19'-butanoyloxyfucoxanthin; FUCO, fucoxanthin; HEX, 19'-hexanoyloxyfucoxanthin; NEO, neoxanthin; PRAS, prasinoxanthin; VIOL, violaxanthin; ALLO, alloxanthin: LUT, lutein; ZEA, zeaxanthin; CHLB, chlorophyll b: CHLA, chlorophyll a.

TABLE 1B Final CHEMTAX pigment ratios.

	PER	BUT	FUCO	HEX	NEO	PRAS	VIOL	ALLO	LUT	ZEA	CHLB	CHLA
Dinoflagellates	0	0	0	0	0.13435	0.13460	0.09189	0	0.00958	0	1.07624	1
Cryptophytes	1.11474	0	0	0	0	0	0	0	0	0	0	1
Cryptophytes	0	0	0	0	0	0	0	0.28313	0	0	0	1
Haptophytes-N	0	0.03260	0.10170	1.24446	0	0	0	0	0	0	0	1
Haptophytes-S	0	0.31029	0.23862	0.56928	0	0	0	0	0	0	0	1
Chlorophytes	0	0	0	0	0.06572	0	0.05983	0	0.17598	0.01075	0.25072	1
Cyanobacteria	0	0	0	0	0	0	0	0	0	0.31681	0	1
Diatoms	0	0	0.75032	0	0	0	0	0	0	0	0	1

Results

Hydrographic features

The location of the Sub-Antarctic (SAF) and Polar (PF) fronts were characterized based on continuous temperature and salinity observations alongside discrete nutrient profiles (Figure 2). The SAF was identified from 171 to 169.5°W, by a drop in temperature from ~9.6°C to 6.5°C. The PF was identified from 165.5 to 161°W by a decrease in a temperature and an increase in silicic acid concentration from 4.02 to 19.39 µM. The Southern Antarctic Circumpolar Current font (sACCf) and Southern Boundary of the Antarctic Circumpolar Current (sbACC) climatological fronts (Orsi et al., 1995) have been overlaid on the transect map in Figure 1, however they were not directly identified in the hydrographic data as their definitions rely on subsurface data.

Pigments

Concentrations of chl-a measured west of 100°W were relatively low, ranging from 0.05 to 0.43 µg/L (Supplementary Figure 1). The highest levels of chl-a (up to 1.57 µg/L) were found at the eastern end of the transect, near the coast of the Western Antarctic Peninsula (WAP). Concurrently, the maximum values for the majority of the other pigments analyzed occurred in the WAP coastal region as well, with the exception of 19'-hexanoyloxyfucoxanthin and zeaxanthin which had maximum values near the north-western end of the transect. Fucoxanthin, the major carotenoid in diatoms had the highest concentration near the eastern end of the transect, correlating strongly with chl-a ($R^2 = 0.91$). However, fucoxanthin is not an unambiguous marker for diatoms, as the pigment is shared with haptophytes. Conversely, 19'-hexanoyloxyfucoxanthin, a pigment found in some haptophytes and chrysophytes, had highest concentrations at the western end of the transect.

CHEMTAX analysis

The contribution of various phytoplankton taxa to total chl-a is illustrated in Figure 3. Diatoms, relatively absent northwest of 140° W, increased towards the east with maximal values near the Antarctic Peninsula. Dinoflagellates, cryptophytes, and haptopytes-S had maximal contributions to chl-a in this region as well. The highest contribution of haptophytes-N to total chl-a were at the northwest end of the transect, decreasing towards the east. Cyanobacteria had peak levels in the north-westerly region as well. Prasinophytes, which were largely absent throughout the middle of the transect, make a small contribution of chl-a near the northwest end of the transect, and around the Antarctic Peninsula.

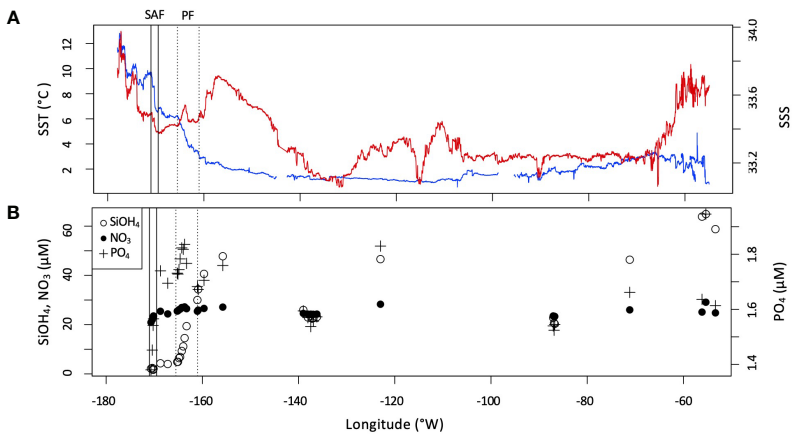

FIGURE 2
(A) Sea surface temperature (SST, blue) and salinity (SSS, red) measured underway across the transect. Ranges of the Sub-Antarctic front (SAF) and Polar front (PF) indicated by solid and dotted vertical bars, respectively. **(B)** Surface nutrient concentrations (NO_3, $SiOH_4$, and PO_4) measured along the transect.

The percent contribution of each taxonomic group to total biomass, by proxy of chl-a, is illustrated in Figure 4A. The dominant taxa west of 160°W were the haptophytes, while diatoms constituted the largest percent of biomass around and east of 160°W. All other taxonomic groups constituted less than 12% of chl-a across the entire transect.

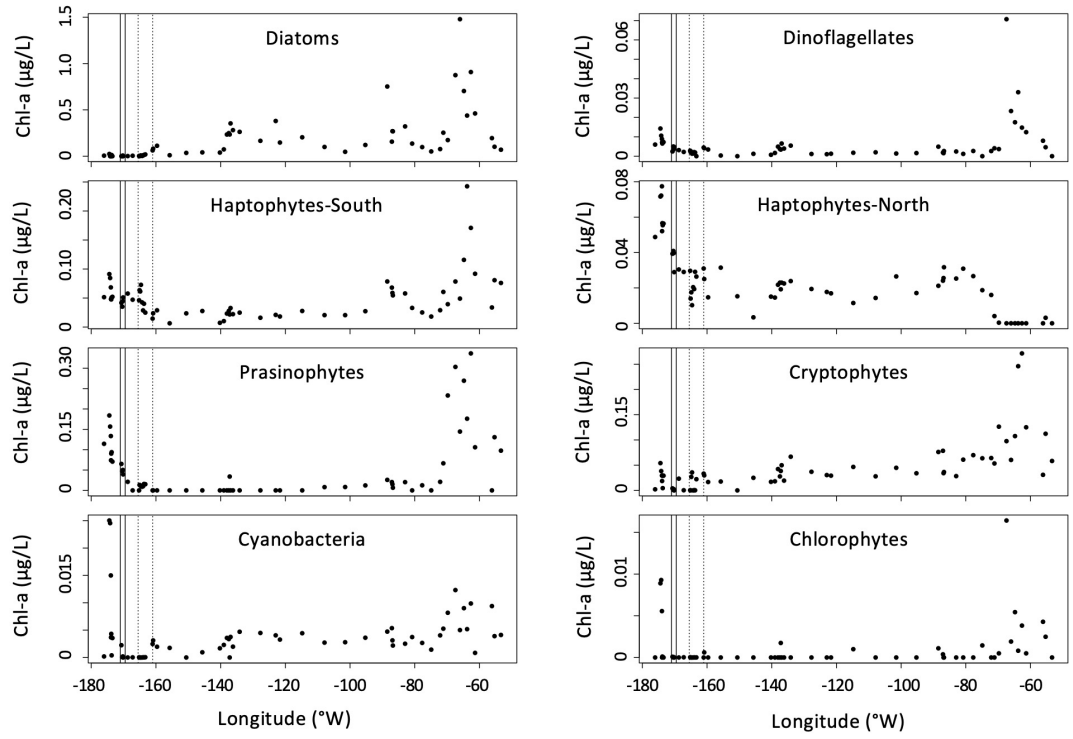

FIGURE 3
CHEMTAX estimates of phytoplankton pigment groups to total chl-a concentrations (µg/L) during the ANA08D 2018 research expedition. The boundaries of the SAF and PF are indicated by solid and dotted vertical lines, respectively.

Mycosporine-like amino acids

HPLC analysis revealed 6 dominant MAAs in this region: porphyra-334, shinorine, palythine, mycosporine-glycine, palythenic-acid, and one MAA that could not be identified using secondary standards (Supplementary Figure 2). The unidentified MAA is referred to in this study as "Unknown". The MAA described as palythenic-acid was identified by an expected mass of 329 *m/z* but was not confirmed with a secondary standard. Small quantities of other MAAs including palythene were detected, however they are not included in this study as the 6 dominant MAAs accounted for more than 95% of the total peak area in all samples analyzed, with the exception of one (81% peak area; 55.55°S, 173.90°W).

MAAs were ubiquitous in all samples analyzed throughout the transect (Figure 4B). Porphyra-334 was the most abundant

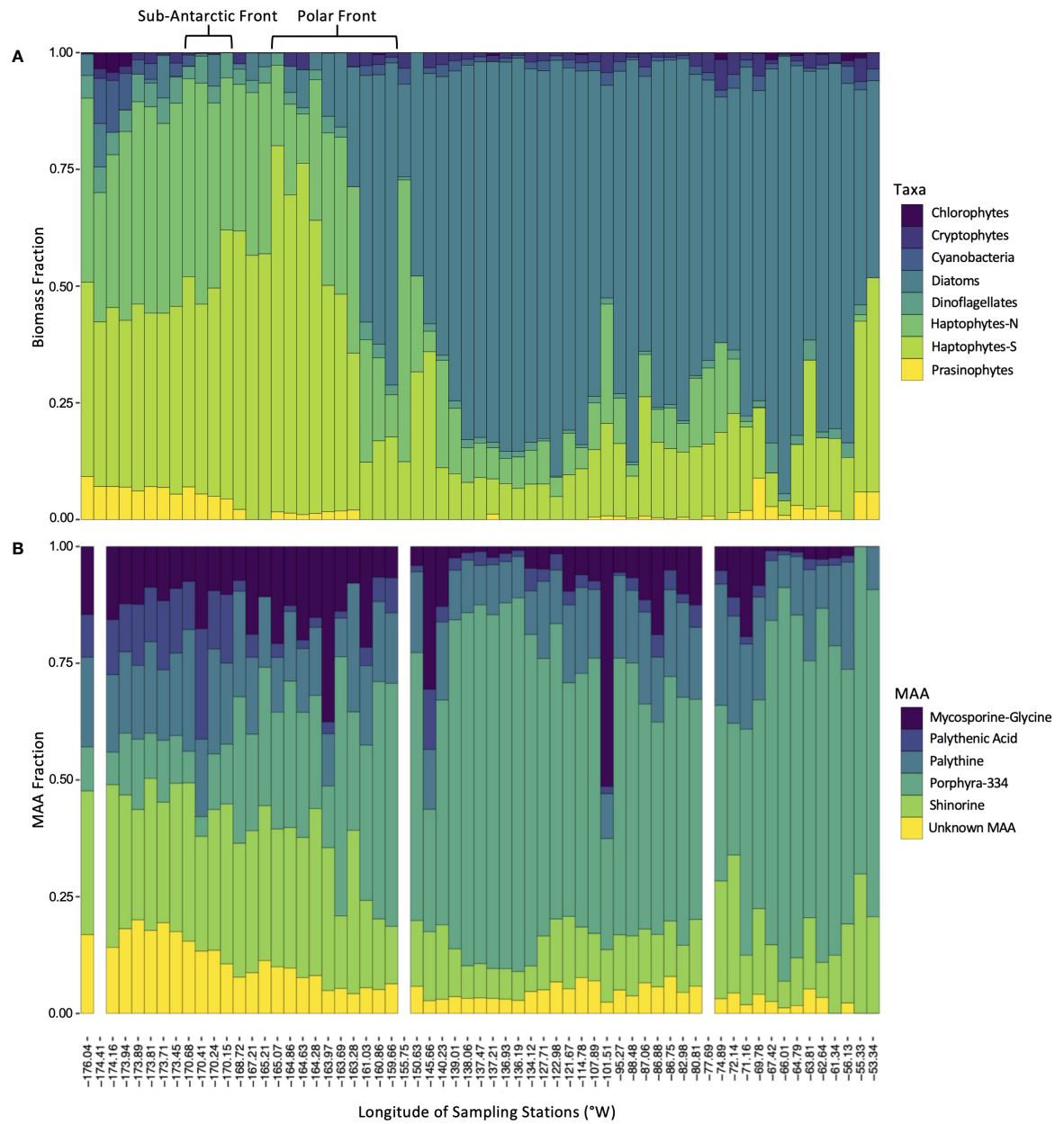

FIGURE 4
Distribution of phytoplankton taxa and mycosporine-like amino acids during ANA08D 2018 research expedition. **(A)** Estimated fraction of each taxonomic group to total biomass. **(B)** Fractional contribution of each dominant MAA to the total MAA pool. Blank columns indicate stations that were not sampled for MAA analysis.

MAA across the transect, with maximum concentrations of > 0.30 µg/L from 139.0104°W to 134.1218°W coinciding with a local MAA:chl-a maximum, and near the coastal region of the WAP at 65.2106°S, 66.0136°W. All other MAAs had relatively similar patterns to one another with maximum values in the northern stations, west of 170°W, however mycosporine-glycine had relatively high concentrations at sporadic sites throughout the transect.

The MAAs northwest of the PF were composed of a relatively even and diverse mixture of MAAs, with shinorine contributing 30.0% ± 4.7 (mean ± SD) of the total MAA pool, followed by palythine contributing 17.2% ± 12.1. Southeast of the PF, porphyra-334 accounted for over 50% of the MAA pool in the majority of samples, with values up to 84.3% (Figure 4B).

The sum of the concentrations of the six dominant MAAs varied by a factor of 200. The highest concentration of MAAs detected was 0.58 µg/L at 55.52°S, 173.94°W, north of the SAF, followed by a cluster of increasing concentrations from 67.35°S, 138.06°W to 67.72°S, 134.12°W (Figure 5A). MAA concentrations normalized to chl-a (MAA:chl-a) decreased from the northwestern end of the transect region to 140°W, and a local maximum of MAA:chl-a was observed from 139.01° W to 134.12°W (Figure 5B). This cluster coincided with an abrupt drop in temperature of ~0.5°C relative to surrounding samples. The lowest values of MAA:chl-a, ~0.01 µg/L, were observed at the end of the transect in coastal waters near the Antarctic peninsula.

A strong positive correlation was found between the diatom fraction of phytoplankton biomass and the porphyra-334 fraction of the MAA pool (R^2 = 0.744, P < 0.0001, Figure 6). All other MAAs were inversely related to the diatom fraction, shinorine being the strongest inverse correlation (R^2 = 0.797, P < 0.0001). Haptophytes-S were most strongly correlated with the shinorine fraction of the MAA pool (R^2 = 0.657, P < 0.0001), whereas haptophytes-N were most strongly correlated with palythenic-acid fraction (R^2 = 0.647, P < 0.0001). Dinoflagellates and prasinophytes were most strongly correlated with the palythenic-acid fraction of the MAA pool as well (R^2 = 0.445, P < 0.0001 and R^2 = 0.363, P < 0.0001, respectively). Chlorophytes, cryptophytes, and cyanobacteria were not significantly correlated with any MAAs in this study.

Modeled UVR dosages

Monthly UVR doses experienced in the sampling region were modeled for January, February, March, and April 2018 (Figure 7A). Satellite data required for modeling was largely irretrievable across the transect in April due to cloud cover and was subsequently excluded from analysis. The strongest UVR doses in the mixed layer were estimated at the highest latitudes, at the western end of the transect. An overall monthly decrease in UVR dosage was observed from February through April due both to seasonal transition and variations in mixed layer depth The strongest, albeit weak correlation between total MAAs and UVR was with UVB (305 nm) in February (R^2 = 0.28). When total MAAs were normalized to chl-a, UVR dosages in both the UVA and UVB (305, 325, 340, and 380 nm) were found to be strongly correlated with UVR dosages observed in February (R^2 = 0.78, 0.58, 0.56, 0.57, respectively; Figure 7B; Supplementary Figure 3).

Discussion

This study highlights the ubiquity of mycosporine-like amino acids across the Southern Ocean in a transect from New Zealand to the Antarctic Peninsula in 2018. This is the first report of the surface-distribution of MAAs across the major Southern Ocean fronts and provides further evidence for the widespread global presence of MAAs suggested by Llewellyn et al. (2012). A linear correlation between the mean daily UVR dosage for the month preceding sampling and MAA:chl-a

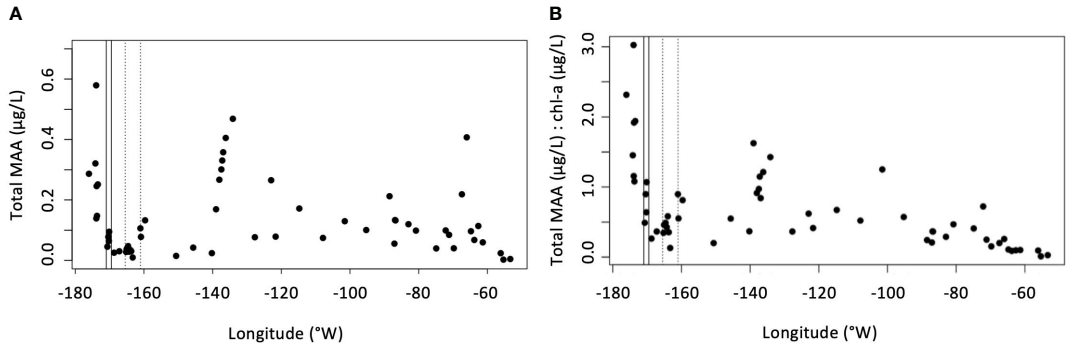

FIGURE 5
(A) Sum of all MAAs (µg/L) across the transect of the ANA08D 2018 research expedition. **(B)** Ratio of sum of all MAAs (µg/L) to chl-a (µg/L) across the transect of the ANA08D 2018 research expedition.

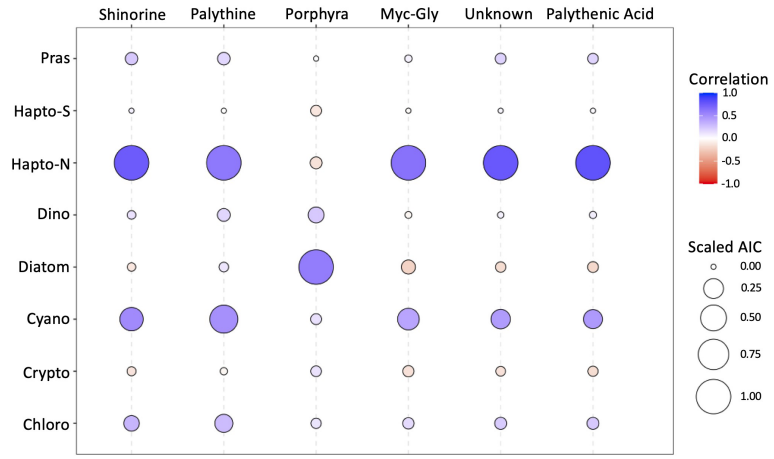

FIGURE 6
Pearson correlation coefficient and scaled Akaike information criterion (AIC) between taxonomic and MAA fractions.

highlights the importance of light history. It has been shown that previous light history plays an important role in development of UVR screening molecules in photosynthetic organisms (Carreto et al., 1989). Llewellyn et al. (2012) found a significant linear correlation between MAA:chl-a and the mean UVR dose in the mixed layer for the month preceding sampling across the

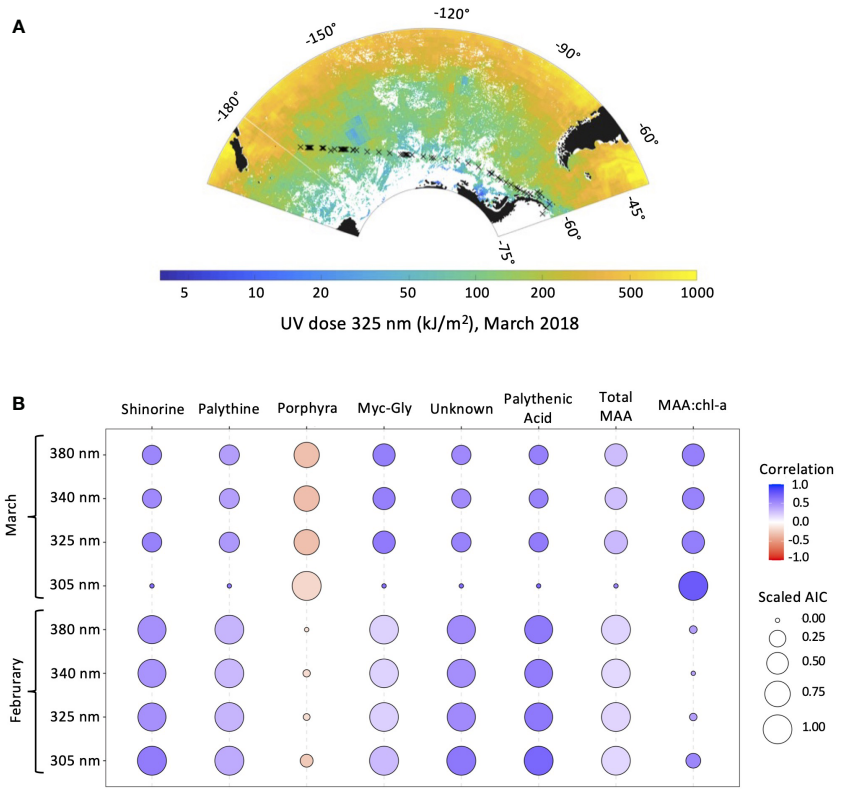

FIGURE 7
(A) Modeled UVR dosage at 325 nm for March 2018 overlaid on cruise transect map. **(B)** Pearson correlation coefficient and scaled Akaike information criterion (AIC) between UVR dosage at 305, 325, 340, and 380 nm in February and March 2018, and MAA fractions, total MAAs, and MAA:chl-a.

Atlantic Ocean, but not during the month of sampling. Unfortunately, due to limited satellite retrievals in our region during April we were unable to obtain UVR doses in the mixed layer for the majority of our sampling sites. However, the significant linear correlation between MAA:chl-a and the mean daily UVR doses calculated for March suggests the results presented by Llewellyn et al. (2012) are consistent for the Southern Ocean as well. While along-track measurements of UVR were obtained, variability in the time of day of sampling and changes in cloud cover rendered comparisons of MAA composition to acute UVR exposure impractical. It should be noted that without field experiments using UVR filters as a control, it is difficult to differentiate the relative contribution of the broader solar spectrum and UVR to MAA concentrations, and that strong correlations were found between sea surface temperature (SST) and MAA:chl-a concentrations in addition to modeled UVR dosage (Supplementary Figure 4). However, SST and UVR were strongly correlated across our transect, as is typical for the marine sea surface (Beckmann et al., 2014).

This study also highlights the relationship between oceanic fronts, phytoplankton taxa and MAA presence in the water column. A parallel study of the bacterioplankton community across oceanic fronts in this region revealed transitions in the prokaryotic composition as a function of environmental gradients and oceanographical discontinuities (Maturana-Martínez et al., 2022). In this study, a distinct transition in phytoplankton taxa was observed across the PF in our transect from haptophytes north of the PF to diatoms south of the PF. The highest levels of MAAs relative to chl-a were present north of the PF, associated with the haptophyte population. While culture isolates of haptophytes have previously been shown to express high levels of MAAs (Jeffrey et al., 1999), this region of the transect was also subjected to the highest modeled levels of daily mean UVR in the month preceding sampling, making it difficult to separate the influence of taxonomy and UVR on MAA:chl-a. A lack of correlation with chlorophytes, cryptophytes, and cyanobacteria to any specific MAA may be due to the low biomass of these taxa present in samples, as chlorophytes, cryptophytes and cyanobacteria in other regions have been shown to possess MAAs, or a lack of production of unique MAAs within these taxa (Llewellyn and Airs, 2010; Rastogi and Incharoensakdi, 2013). Previous laboratory and field studies in the Southern Ocean have highlighted an inverse relationship between taxonomic sensitivity to UVR and presence of photoprotective pigments (Vernet et al., 1994). Biologically significant dosages of UVR can penetrate to depths of at least 2-20 m in the Southern Ocean (Boelen et al., 1999; Smyth, 2011; Núñez-Pons et al., 2018), with attenuation of UVR dependent on the optical properties of the water column (e.g. enhanced absorption of UVR by CDOM, contributing to spatial gradients in absorption and penetration depth from the coastal to open ocean; Häder et al., 2011; Núñez-Pons et al., 2018). This indicatesthat UVR forcing is of relevance inthe UML but not the entirety of the euphotic zone. Recent development of state-of-the-art biogeochemical models capable of resolving phytoplankton metabolism and bio-optics (Dutkiewicz et al., 2015; Casey et al., 2022), in concert with a more detailed understanding of physiological capacity and bio-optical feedbacks across a wider range of phytoplankton taxa, provide an intriguing path forward to quantitatively test this hypothesis and examine links between photobiology and biogeography at basin scales.

The transition to the diatom dominated waters south of the PF coincided with a transition to porphyra-334 as the dominant MAA present in the MAA pool. Previous studies of pure cultures including *Thalassiosira* sp., *Fragilariopsis cylindrus*, and *Corethron criophilum* have identified the presence of porphyra-334 and shinorine as the primary MAAs of Antarctic diatoms (Helbling et al., 1996; Riegger and Robinson, 1997; Hernando et al., 2002). A study conducted in the Sub-Antarctic Zone of Tasmania in 2007 also documented a predominance of porphyra-334 as the dominant MAA in the PF zone, which highlights a consistency in MAA composition in the PF zone across a decade timescale (Oubelkheir et al., 2013). Additionally, sediment cores sampled near this transect (NBP9604 St3 MC8, 61°57′S, 170°03′W) were found to contain diatom frustules enriched with MAAs, primarily porphyra-334, corroborating the dominance of this MAA in diatom populations south of the polar front (Ingalls et al., 2010). With the exception of porphya-334, the abundance of each MAA normalized to chl-a was correlated with UVR-dosage, which is reflected in the correlation between total MAAs to chl-a and UVR-dosage. The lack of correlation between porphyra-334 and UV-dosage observed across our transect may be due to the rapid transition to diatoms containing porphyra-334 at the PF, and subsequent influence of other abiotic stressors south of the PF on MAA quality and quantity, such as nutrient availability (Peinado et al., 2004; Oren and Gunde-Cimerman, 2007).

Diatoms have been used as a diagnostic for the location of the PF due to their dependance on dissolved silica for their siliceous frustules (Barron, 1996; Cortese and Gersonde, 2008). Given the relationship between diatoms, porphyra-334, and silica present at the polar front, porphyra-334 may serve as an alternate proxy for the location of the PF zone. Kahru et al. (2021) demonstrated the ability to differentiate neighboring algal blooms of differing taxonomic composition *via* the remote detection of UVR spectral bands, likely due to the presence of MAAs. However, this differentiation was hypothesized to be based on the presence of the MAA palythene, which has a peak absorption at 360 nm in the long-wavelength UVA region. Given the similarity in absorption spectra between porphyra-334 and the MAAs associated with the haptophyte population north of the PF, distinguishing between the two will likely prove difficult. Furthermore, the challenge to use future satellites to retrieve signals below 350 nm may prove insurmountable due to the strong increase in Rayleigh scattering by the atmosphere at

shorter wavelengths. However future studies in tandem with a complete suite of optical measurements are warranted and certainly could be applied on *in situ* gliders, moorings and profilers.

Here the profile of MAAs in phytoplankton in a transect from Eastern New Zealand to the WAP has been documented for April 2018, however future work should be conducted to document seasonal changes in MAA composition. Concentrations of MAAs have been documented to be highest during summer months in Sub-Antarctic red seaweeds (Jofre et al., 2020), however an inverse phenomenon has been observed in regions with high levels of nutrients during the winter (Briani et al., 2018). Presumably, lower Winter irradiance levels will result in a reduction of MAA:chl-a, and seasonal variations in nutrient availability and phytoplankton taxa composition will result in changes in MAA quantity and quality in this region. As climate change effects range expansion and contraction of varying phytoplankton taxa, baseline measurements will be necessary in order to separate seasonal variability in MAA quantity and composition from anomalies. Notably, blooms of phytoplankton containing MAAs with spectral signatures within the detection range of satellite sensors, such as dinoflagellates, may be detectable in the Southern Ocean by means of remote sensing with improved algorithms extended into the ultraviolet. Additionally, future studies incorporating metagenomics and metatranscriptomics in tandem with MAA analysis will allow for a higher resolution of phytoplankton groups, their correlation with specific MAAs beyond the taxa identified in this study, and an enhanced understanding of their utility as bio-indicators of UVR induced stress.

Conclusion

Amidst climate change and subsequent variations in interactions between phytoplankton and abiotic factors such as UVR, it is important to establish baseline patterns for MAA expression in the world's oceans. With the advent of new hyperspectral remote sensing platforms, a baseline understanding of the global distribution of MAAs will likely enhance capabilities to observe changes in the distribution of MAAs and MAA:chl-a as a proxy for the photoprotective response of phytoplankton. Additionally, an enhanced understanding of the distribution and utility of MAAs to serve as a bio-indicator of UVR-induced stress in phytoplankton may help to improve models that incorporate spectral light and explicit radiative transfer to examine the role of the irradiance spectrum and pigments in establishing biogeography. The results presented here demonstrate a correlation between the preceding month's mean daily UVR dosage and MAA:chl-a, as previously described for the Atlantic Ocean, as well as a shift to a predominance of the MAA porphyra-334 south of the PF, concurrent with a dominant diatom population.

Data availability statement

The raw data supporting the conclusions of this article will be made available by the authors, without undue reservation.

Author contributions

EW, MC, MV, S-YH, BM, and JI contributed to the study conception and design. Sample preparation was performed by MC, BP, JI, and S-YH. Data collection was performed by MC, BP, JI, S-YH, and TS. Sample analysis was performed by EW. Statistical analysis was performed by EW and CJ. The first draft of the manuscript was written by EW and all authors commented on subsequent versions of the manuscript. All authors contributed to the article and approved the submitted version.

Funding

This research was conducted as a part of the project Carbon cycle change and ecosystem response under the Southern Ocean warming (PE22110) and supported by the Korea Polar Research Institute (KOPRI), Incheon. ELW was funded by the National Science Foundation through GRFP DGE-1650112 and MV was supported by the National Science Foundation Office of Polar Programs through award number 1822289. The research was also carried out at the Jet Propulsion Laboratory, California Institute of Technology, under a contract with the National Aeronautics and Space Administration (80NM0018D0004).

Acknowledgments

We thank the Araon crew and captain for their assistance and logistical support. We also thank Michael Lesser and Kai Bishoff for isolating and providing MAA secondary standards.

Conflict of interest

The authors declare that the research was conducted in the absence of any commercial or financial relationships that could be construed as a potential conflict of interest.

Publisher's note

reviewers. Any product that may be evaluated in this article, or claim that may be made by its manufacturer, is not guaranteed or endorsed by the publisher.

Supplementary material

The Supplementary Material for this article can be found online at: https://www.frontiersin.org/articles/10.3389/fmars.2022.1022957/full#supplementary-material

SUPPLEMENTARY FIGURE 1
Concentration of all pigments (µg/L) analyzed by HPLC along the transect plotted with respect to longitude. The boundaries of the SAF and PF are indicated by solid and dotted vertical lines, respectively.

SUPPLEMENTARY FIGURE 2
Representative HPLC chromatograms of MAA samples from extracts. **(A)** North of the PF, latitude -55.38°S, longitude -174.16°W, and **(B)** South of the PF, latitude -67.72°S, longitude -134.12°W. MAAs identified in the chromatogram were 1) shinorine, λ_{max} 332, retention time 5.4 min; 2) palythine λ_{max} 319 nm, retention time 8.8 min; 3) porphyra-334 λ_{max} 332 nm, retention time 10.5 min; 4) mycosporine-glycine, λ_{max} 309 nm, retention time 12.2 min; 5) Unknown MAA, λ_{max} 334 nm, retention time 18.1 min; 6) palythenic-acid, λ_{max} 336 nm, retention time 20.5 min.

SUPPLEMENTARY FIGURE 3
Scatter plots of modeled UVR dosages for March 2018 versus MAA:chl-a. **(A)** UVR dosage at 305 nm versus MAA:chl-a. **(B)** UVR dosage at 325 nm versus MAA:chl-a.

SUPPLEMENTARY FIGURE 4
Pearson correlation coefficients between abiotic factors.

References

Barnes, P. W., Williamson, C. E., Lucas, R. M., Robinson, S. A., Madronich, S., Paul, N. D., et al. (2019). Ozone depletion, ultraviolet radiation, climate change and prospects for a sustainable future. *Nat. Sustain.* 2, 569–579. doi: 10.1038/s41893-019-0314-2

Barron, J. A. (1996). Diatom constraints on the position of the Antarctic polar front in the middle part of the pliocene. *Mar. Micropaleontol.* 27, 195–213. doi: 10.1016/0377-8398(95)00060-7

Beckmann, M., Václavík, T., Manceur, A. M., Šprtová, L., von Wehrden, H., Welk, E., et al. (2014). glUV: A global UV-b radiation data set for macroecological studies. *Methods Ecol. Evol.* 5, 372–383. doi: 10.1111/2041-210X.12168

Boelen, P., Obernostere, I., Vink, A. A., and Buma, A. G. J. (1999). Attenuation of biologically effective UV radiation in tropical Atlantic waters measured with a biochemical DNA dosimeter. *Photochem. Photobiol.* 69, 34–40. doi: 10.1111/j.1751-1097.1999.tb05303.x

Briani, B., Sissini, M. N., Lucena, L. A., Batista, M. B., Costa, I. O., Nunes, J. M. C., et al. (2018). The influence of environmental features in the content of mycosporine-like amino acids in red marine algae along the Brazilian coast. *J. Phycol.* 54, 380–390. doi: 10.1111/jpy.12640

Carreto, J. I., and Carignan, M. O. (2011). Mycosporine-like amino acids: Relevant secondary metabolites. chemical and ecological aspects. *Mar. Drugs* 9, 387–446. doi: 10.3390/md9030387

Carreto, J. I., Carignan, M. O., and Montoya, N. G. (2005). A high-resolution reverse-phase liquid chromatography method for the analysis of mycosporine-like amino acids (MAAs) in marine organisms. *Mar. Biol.* 146, 237–252. doi: 10.1007/s00227-004-1447-y

Carreto, J. I., Carignan, M. O., Montoya, N. G., Cozzolino, E., and Akselman, R. (2018). Mycosporine-like amino acids and xanthophyll-cycle pigments favour a massive spring bloom development of the dinoflagellate prorocentrum minimum in grande bay (Argentina), an ozone hole affected area. *J. Mar. Syst.* 178, 15–28. doi: 10.1016/j.jmarsys.2017.10.004

Carreto, J. I., De Marco, S. G., and Lutz, V. A. (1989). UV-Absorbing pigments in the dinoflagellates alexandrium excavatum and prorocentrum micans. effects of light intensity. *Red. Tides Biol. Environ. Sci. Toxicol.* 37–40, 333–336. Available at: https://www.researchgate.net/profile/Jose-Carreto/publication/264195513_CARRETO_JI_SG_DE_MARCO_y_VA_LUTZ1989_UV_Absorbing_pigments_in_the_dinoflagellates_Alexandrium_excavatum_and_Prorocentrum_micans_Effects_of_light_intensity_En_Red_Tides_Biology_Environmntal_Science_and/links/53d1726f0cf228d363e65040/CARRETO-JI-SG-DE-MARCO-y-VA-LUTZ1989-UV-Absorbing-pigments-in-the-dinoflagellates-Alexandrium-excavatum-and-Prorocentrum-micans-Effects-of-light-intensity-En-Red-Tides-Biology-Environmntal-Science-a.pdf

Casey, J. R., Boiteau, R. M., Engqvist, M. K. M., Finkel, Z. V., Li, G., Liefer, J., et al. (2022). Basin-scale biogeography of marine phytoplankton reflects cellular-scale optimization of metabolism and physiology. *Sci. Adv.* 8, eabl4930. doi: 10.1126/sciadv.abl4930

Constable, A. J., Melbourne-Thomas, J., Corney, S. P., Arrigo, K. R., Barbraud, C., Barnes, D. K. A., et al. (2014). Climate change and southern ocean ecosystems I: how changes in physical habitats directly affect marine biota. *Glob. Change Biol.* 20, 3004–3025. doi: 10.1111/gcb.12623

Cordero, R. R., Feron, S., Damiani, A., Redondas, A., Carrasco, J., Sepúlveda, E., et al. (2022). Persistent extreme ultraviolet irradiance in Antarctica despite the ozone recovery onset. *Sci. Rep.* 12, 1–10. doi: 10.1038/s41598-022-05449-8

Cortese, G., and Gersonde, R. (2008). Plio/Pleistocene changes in the main biogenic silica carrier in the southern ocean, Atlantic sector. *Mar. Geol.* 252, 100–110. doi: 10.1016/j.margeo.2008.03.015

Cullen, J. J., and Neale, P. J. (1994). Ultraviolet radiation, ozone depletion, and marine photosynthesis. *Photosynth. Res.* 39, 303–320. doi: 10.1007/BF00014589

de Boyer Montégut, C., Madec, G., Fischer, A. S., Lazar, A., and Iudicone, D. (2004). Mixed layer depth over the global ocean: An examination of profile data and a profile-based climatology. *J. Geophys. Res. Ocean.* 109, C12003. doi: 10.1029/2004JC002378

De Mora, S., Demers, S., and Vernet, M. (2000). The effects of UV radiation in the marine environment. Cambridge: Cambridge University Press. 10. doi: 10.1017/CBO9780511535444

Dutkiewicz, S., Hickman, A. E., Jahn, O., Gregg, W. W., Mouw, C. B., and Follows, M. J. (2015). Capturing optically important constituents and properties in a marine biogeochemical and ecosystem model. *Biogeosciences* 12, 4447–4481. doi: 10.5194/bg-12-4447-2015

Erickson, D. J., Sulzberger, B., Zepp, R. G., and Austin, A. T. (2015). Effects of stratospheric ozone depletion, solar UV radiation, and climate change on biogeochemical cycling: Interactions and feedbacks. *Photochem. Photobiol. Sci.* 14, 127–148. doi: 10.1039/c4pp90036g

Fahey, D., Newman, P. A., Pyle, J. A., Safari, B., Chipperfield, M. P., Karoly, D., et al. (2018). *Scientific assessment of ozone depletion: 2018, global ozone research and monitoring project-report no. 58*. Geneva, Switzerland: World Meteorological Organization.

Fang, X., Park, S., Saito, T., Tunnicliffe, R., Ganesan, A. L., Rigby, M., et al. (2019). Rapid increase in ozone-depleting chloroform emissions from China. *Nat. Geosci.* 12, 89–93. doi: 10.1038/s41561-018-0278-2

Häder, D. P., and Gao, K. (2015). Interactions of anthropogenic stress factors on marine phytoplankton. *Front. Environ. Sci.* 3. doi: 10.3389/fenvs.2015.00014

Häder, D.-P., Helbling, E. W., Williamson, C. E., and Worrest, R. C. (2011). Effects of UV radiation on aquatic ecosystems and interactions with climate change. *Photochem. Photobiol. Sci.* 10, 242. doi: 10.1039/c0pp90036b

Häder, D.-P., Williamson, C. E., Wängberg, S.-Å., Rautio, M., Rose, K. C., Gao, K., et al. (2015). Effects of UV radiation on aquatic ecosystems and interactions with other environmental factors. *Photochem. Photobiol. Sci.* 14, 108–126. doi: 10.1039/C4PP90035A

Ha, S. Y., Min, J. O., Joo, H. M., Kim, M. S., Kang, S. H., and Shin, K. H. (2018). Synthesis of mycosporine-like amino acids by a size-fractionated marine phytoplankton community of the arctic beaufort sea. *J. Photochem. Photobiol. B. Biol.* 188, 87–94. doi: 10.1016/j.jphotobiol.2018.09.008

Harris, N. R. P., Montzka, S. A., Newman, P. A.others (2019). Report on the international symposium on the unexpected increase in emissions of ozone-depleting CFC-11. *SPARC. Newsl.* 53, 9–18. Available at: https://www.sparc-climate.org/wp-content/uploads/sites/5/2019/07/SPARCnewsletter_July2019_WEB.pdf

Helbling, E. W., Chalker, B. E., Dunlap, W. C., Holm-Hansen, O., and Villafañe, V. E. (1996). Photoacclimation of Antarctic marine diatoms to solar ultraviolet radiation. *J. Exp. Mar. Bio. Ecol.* 204, 85–101. doi: 10.1016/0022-0981(96)02591-9

Hernando, M., Carreto, J. I., Carignan, M. O., Ferreyra, G. A., and Gross, C. (2002). "Effects of solar radiation on growth and mycosporine-like amino acids

content in thalassiosira sp, an Antarctic diatom," In: W. E. Arntz and A. Clarke (eds) *Ecological studies in the Antarctic Sea ice zone* (Berlin, Heidelberg: Springer), 237–245. doi: 10.1007/978-3-642-59419-9_31

Hessen, D. O. (1993). DNA-Damage and pigmentation in alpine and arctic zooplankton as bioindicators of UV-radiation. *SIL. Proc. 1922-2010.* 25, 482–486. doi: 10.1080/03680770.1992.11900171

Hood, E., Fellman, J. B., and Spencer, R. G. M. (2020). Glacier loss impacts riverine organic carbon transport to the ocean. *Geophys. Res. Lett.* 47, 0–3. doi: 10.1029/2020GL089804

Hood, E. M., Sabine, C. L., and Sloyan, B. M. eds. (2010). The GO-SHIP repeat hydrography manual: A collection of expert reports and guidelines. *IOCCP Report Number 14*, ICPO Publication Series Number 134. Available online at http://www.go-ship.org/HydroMan.html

Hydes, D., Aoyama, M., Aminot, A., Bakker, K., Becker, S., Coverly, S., et al. (2010). Determination of dissolved nutrients (N, P, Si) in seawater with high precision and inter-comparability using gas-segmented continuous flow analysers. *Go-sh. Repeat Hydrogr. Man. IOCCP Rep*. 134, 1–87. Available at: http://archimer.ifremer.fr/doc/00020/13141/.

Ingalls, A. E., Whitehead, K., and Bridoux, M. C. (2010). Tinted windows: The presence of the UV absorbing compounds called mycosporine-like amino acids embedded in the frustules of marine diatoms. *Geochim. Cosmochim. Acta* 74, 104–115. doi: 10.1016/j.gca.2009.09.012

Jeffrey, S. W., MacTavish, H. S., Dunlap, W. C., Vesk, M., and Groenewoud, K. (1999). Occurrence of UVA-and UVB-absorbing compounds in 152 species (206 strains) of marine microalgae. *Mar. Ecol. Prog. Ser.* 189, 35–51. doi: 10.3354/meps189035

Jofre, J., Celis-Plá, P. S. M., Figueroa, F. L., and Navarro, N. P. (2020). Seasonal variation of mycosporine-like amino acids in three subantarctic red seaweeds. *Mar. Drugs* 18, 1–17. doi: 10.3390/md18020075

Kahru, M., Anderson, C., Barton, A. D., Carter, M. L., Catlett, D., Send, U., et al. (2021). Satellite detection of dinoflagellate blooms off California by UV reflectance ratios. *Elem. Sci. Anthr.* 9, 00157. doi: 10.1525/elementa.2020.00157

Kahru, M., and Mitchell, B. G. (1998). Spectral reflectance and absorption of a massive red tide off southern California. *J. Geophys. Res. Ocean.* 103, 21601–21609. doi: 10.1029/98JC01945

Latasa, M. (2007). Improving estimations of phytoplankton class abundances using CHEMTAX. *Mar. Ecol. Prog. Ser.* 329, 13–21. doi: 10.3354/meps329013

Lee, Z. P., Darecki, M., Carder, K. L., Davis, C. O., Stramski, D., and Rhea, W. J. (2005). Diffuse attenuation coefficient of downwelling irradiance: An evaluation of remote sensing methods. *J. Geophys. Res. Ocean.* 110, 1–9. doi: 10.1029/2004JC002573

Lesser, M. P. (1996). Acclimation of phytoplankton to UV-b radiation: oxidative stress and photoinhibition of photosynthesis are not prevented by UV-absorbing compounds in the dinoflagellate prorocentrum micans. *Mar. Ecol. Prog. Ser.* 132, 287–297. doi: 10.3354/meps132287

Llewellyn, C. A., and Airs, R. L. (2010). Distribution and abundance of MAAs in 33 species of microalgae across 13 classes. *Mar. Drugs* 8, 1273–1291. doi: 10.3390/md8041273

Llewellyn, C. A., Greig, C., Silkina, A., Kultschar, B., Hitchings, M. D., and Farnham, G. (2020). Mycosporine-like amino acid and aromatic amino acid transcriptome response to UV and far-red light in the cyanobacterium chlorogloeopsis fritschii PCC 6912. *Sci. Rep.* 10, 1–13. doi: 10.1038/s41598-020-77402-6

Llewellyn, C. A., and Harbour, D. S. (2003). A temporal study of mycosporine-like amino acids in surface water phytoplankton from the English channel and correlation with solar irradiation. *J. Mar. Biol. Assoc. United. Kingdom.* 83, 1–9. doi: 10.1017/S0025315403006726h

Llewellyn, C. A., White, D. A., Martinez-Vincente, V., Tarran, G., and Smyth, T. J. (2012). Distribution of mycosporine-like amino acids along a surface water meridional transect of the Atlantic. *Microb. Ecol.* 64, 320–333. doi: 10.1007/s00248-012-0038-6

Mackey, M. D., Mackey, D. J., Higgins, H. W., and Wright, S. W. (1996). CHEMTAX-a program for estimating class abundances from chemical markers: application to HPLC measurements of phytoplankton. *Mar. Ecol. Prog. Ser.* 144, 265–283. doi: 10.3354/meps144265

Maturana-Martínez, C., Iriarte, J. L., Ha, S.-Y., Lee, B., Ahn, I.-Y., Vernet, M., et al. (2022). Biogeography of southern ocean active prokaryotic communities over a Large spatial scale. *Front. Microbiol.* 13. doi: 10.3389/fmicb.2022.862812

Moisan, T. A., and Mitchell, B. G. (2001). UV Absorption by mycosporine-like amino acids in phaeocystis antarctica Karsten induced by photosynthetically available radiation. *Mar. Biol.* 138, 217–227. doi: 10.1007/s002270000424

Morrison, J. R., and Nelson, N. B. (2004). Seasonal cycle of phytoplankton UV absorption at the Bermuda Atlantic time-series study (BATS) site. *Limnol. Oceanogr.* 49, 215–224. doi: 10.4319/lo.2004.49.1.0215

Núñez-Pons, L., Avila, C., Romano, G., Verde, C., and Giordano, D. (2018). UV-Protective compounds in marine organisms from the southern ocean. *Mar. Drugs* 16, 336. doi: 10.3390/md16090336

Oren, A., and Gunde-Cimerman, N. (2007). Mycosporines and mycosporine-like amino acids: UV protectants or multipurpose secondary metabolites? *FEMS Microbiol. Lett.* 269, 1–10. doi: 10.1111/j.1574-6968.2007.00650.x

Orfanoudaki, M., Hartmann, A., Karsten, U., and Ganzera, M. (2019). Chemical profiling of mycosporine-like amino acids in twenty-three red algal species. *J. Phycol.* 55, 393–403. doi: 10.1111/jpy.12827

Orsi, A. H., Whitworth, T., and Nowlin, W. D. (1995). On the meridional extent and fronts of the Antarctic circumpolar current. *Deep. Res. Part I.* 42, 641–673. doi: 10.1016/0967-0637(95)00021-W

Oubelkheir, K., Clementson, L. A., Moore, G. F., and Tilstone, G. H. (2013). Production of mycosporine-like amino acids by phytoplankton under ultraviolet radiation exposure in the Sub-Antarctic zone south of Tasmania. *Mar. Ecol. Prog. Ser.* 494, 41–63. doi: 10.3354/meps10530

Peinado, N. K., Abdala Díaz, R. T., Figueroa, F. L., and Helbling, E. W. (2004). Ammonium and UV radiation stimulate the accumulation of mycosporine-like amino acids in porphyra columbina (Rhodophyta) from Patagonia, Argentina. *J. Phycol.* 40, 248–259. doi: 10.1046/j.1529-8817.2004.03013.x

Portwich, A., and Garcia-Pichel, F. (1999). Ultraviolet and osmotic stresses induce and regulate the synthesis of mycosporines in the cyanobacterium chlorogloeopsis PCC 6912. *Arch. Microbiol.* 172, 187–192. doi: 10.1007/s002030050759

Rastogi, R. P., and Incharoensakdi, A. (2013). UV Radiation-induced accumulation of photoprotective compounds in the green alga tetraspora sp. CU2551. *Plant Physiol. Biochem.* 70, 7–13. doi: 10.1016/j.plaphy.2013.04.021

Rastogi, R. P., and Incharoensakdi, A. (2014). UV Radiation-induced biosynthesis, stability and antioxidant activity of mycosporine-like amino acids (MAAs) in a unicellular cyanobacterium gloeocapsa sp. CU2556. *J. Photochem. Photobiol. B. Biol.* 130, 287–292. doi: 10.1016/j.jphotobiol.2013.12.001

Riegger, L., and Robinson, D. (1997). Photoinduction of UV-absorbing compounds in Antarctic diatoms and phaeocystis antarctica. *Mar. Ecol. Prog. Ser.* 160, 13–25. doi: 10.3354/meps160013

Sallée, J. B., Pellichero, V., Akhoudas, C., Pauthenet, E., Vignes, L., Schmidtko, S., et al. (2021). Summertime increases in upper-ocean stratification and mixed-layer depth. *Nature* 591, 592–598. doi: 10.1038/s41586-021-03303-x

Schmid, D., Schuerch, C., and Zuelli, F. (2004). Harmless, natural cosmetic skin treatment compositions, for protecting against UV-a induced lipid oxidation and premature aging, containing mycosporine-like amino acids. *Pat. number. EPI. 1473028-AL*. Available at: https://patentimages.storage.googleapis.com/8b/63/f3/0acf0e6e3a5011/EP1473028A1.pdf

Shick, J. M., and Dunlap, W. C. (2002). Mycosporine-like amino acids and related gadusols: biosynthesis, accumulation, and UV-protective functions in aquatic organisms. *Annu. Rev. Physiol.* 64, 223–262. doi: 10.1146/annurev.physiol.64.081501.155802

Sinha, R. P., Singh, S. P., and Häder, D.-P. (2007). Database on mycosporines and mycosporine-like amino acids (MAAs) in fungi, cyanobacteria, macroalgae, phytoplankton and animals. *J. Photochem. Photobiol. B. Biol.* 89, 29–35. doi: 10.1016/j.jphotobiol.2007.07.006

Smyth, T. J. (2011). Penetration of UV irradiance into the global ocean. *J. Geophys. Res.* 116, C11020. doi: 10.1029/2011JC007183

Vernet, M., Brody, E. A., Holm-Hansen, O., and Mitchell, B. G. (1994). The response of Antarctic phytoplankton to ultraviolet radiation: Absorption, photosynthesis, and taxonomic composition. *Antarct. Res. Ser* 62, 143–158. doi: 10.1029/ar062p0143

Vincent, W. F., and Neal, P. J. (2000). "Mechanisms of UV damage to aquatic organisms," in *The effects of UV radiation in the marine environment*. Cambridge, UK: Cambridge Environmental Chemistry Series; University Press. 149–176.

Wada, N., Sakamoto, T., and Matsugo, S. (2015). Mycosporine-like amino acids and their derivatives as natural antioxidants. *Antioxid. (Basel. Switzerland).* 4, 603–646. doi: 10.3390/antiox4030603

Whitehead, K., and Vernet, M. (2000). Influence of mycosporine-like amino acids (MAAs) on UV absorption by particulate and dissolved organic matter in la Jolla bay. *Limnol. Oceanogr.* 45, 1788–1796. doi: 10.4319/lo.2000.45.8.1788

World Meteorological Organization (WMO) (2018). Executive summary: Scientific assessment of ozone depletion: 2018. *Glob. Ozone. Res. Monit. Proj.* Report No. 58, 67. Geneva, Switzerland. Available at: https://csl.noaa.gov/assessments/ozone/2018/executivesummary/

Wright, S. W., Thomas, D. P., Marchant, H. J., Higgins, H. W., Mackey, M. D., and Mackey, D. J. (1996). Analysis of phytoplankton of the Australian sector of the

southern ocean: Comparisons of microscopy and size frequency data with interpretations of pigment HPLC data using the "CHEMTAX" matrix factorisation program. *Mar. Ecol. Prog. Ser.* 144, 285–298. doi: 10.3354/meps144285

Zapata, M., Rodríguez, F., and Garrido, J. L. (2000). Separation of chlorophylls and carotenoids from marine phytoplankton: A new HPLC method using a reversed phase C8 column and pyridine-containing mobile phases. *Mar. Ecol. Prog. Ser.* 195, 29–45. doi: 10.3354/meps195029